SWIFT XRT CALDB RELEASE NOTE

SWIFT-XRT-CALDB-09:

Response matrices and Ancillary Response Files

Table P1: Files to be released:

Filename[†]	Mode	Grade	Substrate[‡] voltage (V)	Release Date
swxwt0to2s0_20010101v012.rmf	WT	$0 - 2$	0	2013-Mar-13
swxwt0s0_20010101v012.rmf	WT	0	0	2013-Mar-13
swxpc0to12s0_20010101v012.rmf	PC	$0 - 12$	0	2013-Mar-13
swxpc0s0_20010101v012.rmf	PC	0	0	2013-Mar-13
swxwt0to2s0_20070101v012.rmf	WT	$0 - 2$	0	2013-Mar-13
swxwt0s0_20070101v012.rmf	WT	0	0	2013-Mar-13
swxpc0to12s0_20070101v012.rmf	PC	$0 - 12$	0	2013-Mar-13
swxpc0s0_20070101v012.rmf	PC	0	0	2013-Mar-13
swxs0_20010101v001.arf*	PC & WT	–	0	2013-Mar-13

[†] $V_{ss} = 0$ V RMFs containing 20010101 in their names are used on data taken from 2004-Dec-01 to 2006-Dec-31, while those containing 20070101 are used from 2007-Jan-01 to 2007-Aug-30.

[‡] The substrate voltage was permanently raised from $V_{ss} = 0$ V to $V_{ss} = 6$ V on 2007-Aug-30 (see below).

* Unified ARF for both WT and PC modes for data taken from 2004-Dec-01 to 2007-Aug-30.

Scope of Document

This note describes the release of updated *Swift*-XRT Windowed Timing (WT) and Photon Counting (PC) mode redistribution matrix files (RMFs) and ancillary response files (ARFs), appropriate for data taken before the CCD substrate voltage change on 2007-Aug-30 — i.e. for $V_{ss} = 0\,\text{V}$ data (see table P1).

Introduction

The XRT effective area is made up of three main components: the mirror effective area, the filter transmission and the CCD quantum efficiency (QE). The QE is included directly in the redistribution matrix files (RMFs) while the ancillary response files (ARFs) contain the mirror effective area and the filter transmission.

Observation-specific ARF files are produced by the XRTMKARF task (part of the XRTDAS-HEADAS software). This task corrects the nominal (on-axis, infinite extraction region) ARF file from the CALDB for the effects of telescope vignetting and, optionally (*psfflag=yes*), for PSF losses incurred when finite sized extraction regions are used in point source analysis. Additional corrections for CCD defects (caused by 'bad columns' or 'hot-pixels') can be made with the inclusion of an exposure map (with the option *expofile=filename.img*), which can automatically be generated by the data analysis pipeline. The task can also generate ARFs for extended sources (option *extended=yes*), such as clusters of galaxies or supernova remnants.

As well as accounting for the CCD QE, the RMFs model the response of the detector to incident X-rays and are mode, grade and epoch dependent.

Epoch Dependent RMFs

The XRT suffered a thermoelectric cooler power supply failure shortly after launch which meant the CCD could not be operated at the expected nominal temperature of $-100\,^{\circ}\text{C}$. However, by carefully controlling the spacecraft pointing during pre-planned science observations the CCD can be passively cooled to acceptable temperatures in the range $\sim -75\,\text{to}-50\,^{\circ}\text{C}$ (Kennea et al. 2005, SPIE, 5898, 329).

Furthermore, laboratory testing showed that by raising the CCD substrate voltage from $V_{ss} = 0\,\text{V}$ to $V_{ss} = 6\,\text{V}$ the thermally induced dark current in the CCD could be reduced, allowing the CCD to operate a few degrees warmer before excessive hot pixels compromise data quality and telemetry (Godet et al., 2009, A&A, 494, 775). Because of this, the XRT CCD substrate voltage was permanently raised to $V_{ss} = 6\,\text{V}$ on 2007-Aug-30 (at 14:28UT).

A side effect of increasing the substrate voltage in this way is that it caused the CCD depletion depth to decrease slightly which, in turn, altered the QE at high energies and just below the Si edge ($\sim 1.5 - 1.84\,\text{keV}$). This warranted the release of response calibration files specific to the different substrate operating voltages.

Over time, the accumulated radiation dose and high-energy proton interactions cause damage to the CCD (in the imaging area, the store frame area and the serial register) resulting in a build-up of charge traps (i.e. faults in the Si crystalline structure of the CCD which hold onto some of the charge released during an X-ray interaction). The deepest traps are responsible for the strongest line FWHM degradation, with the line shape then showing a more pronounced low energy wing. The most serious of these charge traps can cause a loss of up to $\sim 600\,\text{eV}$ at $6\,\text{keV}$ and $\sim 300\,\text{eV}$ at $1.856\,\text{keV}$ from the incident X-ray energy, although typical values are very much smaller.

For observations taken after 2007-Sep-01, we have mapped the location and depths of the deepest traps on the CCD and updated the *Swift*-XRT XRTCALCPI software task to provide a trap specific energy scale reconstruction (see the gain file release note SWIFT-XRT-CALDB-04_v10 and later for details and caveats). The application of such trap corrections help to restore the spectral resolution (FWHM) of the detector — improvements in FWHM from 175 eV in PC (225 eV in WT) at 1.86 keV in early 2010 to approximately 130 eV (for both modes) are seen; this level has subsequently been maintained with further updates to the gain files.

Both the change in substrate voltage and degradation in spectral resolution (up to the point at which trap corrections have been enabled) necessitate the release of RMFs with different QEs and kernel broadening depending on the epoch of the observation.

Motivation behind this release

This release is the first to provide new RMFs generated by an improved CCD22 modelling code, which has been under development for the last 18 months. It also provides an updated ARF, derived from new mirror area file computations (including the effects of a thin hydrocarbon coating) and optical blocking filter transmission curve modelling. **In this release, updated WT and PC RMFs and ARFs are made available appropriate for** $V_{ss} = 0$ V **observations — i.e. those taken before 2007-Aug-31.** (Note, the current $V_{ss} = 6$ V calibration is described in the previous release note SWIFT-XRT-CALDB-09_v16.)

These RMFs supersede the $V_{ss} = 0$ V v011 PC RMFs (released on 2008-May-09 and 2009-Dec-03, described in release notes SWIFT-XRT-CALDB-09_v11 and SWIFT-XRT-CALDB-09_v13) and the v011 WT RMFs (released on 2008-May-09 and 2009-Apr-07, release notes SWIFT-XRT-CALDB-09_v11 and SWIFT-XRT-CALDB-09_v12). The ARF supersedes the $V_{ss} = 0$ V v011 files released 2008-May-09 (release note SWIFT-XRT-CALDB-09_v11).

RMF/ARF file naming scheme

The change in substrate voltage made it necessary to release two sets of RMF/ARF files, distinguished by the characters 's0' and 's6' in their filenames. The filenames also encode the XRT readout mode (WT or PC), the grade selection ($0 - 2$ or 0 for WT; $0 - 12$ or 0 for PC) and the epoch the files are valid for use from.

The RMFs released this time are, for WT mode:

grade $0 - 2$	grade 0
swxwt0to2s0_20010101v012.rmf	swxwt0s0_20010101v012.rmf [†]
swxwt0to2s0_20070101v012.rmf	swxwt0s0_20070101v012.rmf

and for PC mode :

grade $0 - 12$	grade 0
swxpc0to12s0_20010101v012.rmf	swxpc0s0_20010101v012.rmf [†]
swxpc0to12s0_20070101v012.rmf	swxpc0s0_20070101v012.rmf

([†] Note, whilst all scientifically interesting $V_{ss} = 0$ V data were taken after XRT first light on 2004-Dec-11 and before the permanent switch to $V_{ss} = 6$ V operation on 2007-Aug-30, the filename epoch predates this to account for $V_{ss} = 0$ V ground calibration data taken before launch.)

A common ARF is now available, valid for both modes, all grade selections and throughout the $V_{ss} = 0$ V epoch :

swxs0_20010101v001.arf

The RMFs are located in the HEASARC CALDB under the directory $CALDB/data/swift/xrt/cpf/rmf and the ARF under $CALDB/data/swift/xrt/cpf/arf.

A complete summary of all RMFs/ARFs presently in use can be found in table A1.

Detailed Description

Redistribution Matrix Files

The *Swift*-XRT X-ray detector is a CCD22 device produced by e2v and is the same type of CCD used in the *XMM-Newton* EPIC MOS cameras. The CCD Response Matrix Files (RMFs) are created by a newly rewritten Monte-Carlo simulation code. Godet et al. (2009, A&A, 494, 775 and references therein), described the previous version of the code, though many of the details written there are still applicable to the new code.

As with previous versions, the new code models the following : the transmission of the incident X-rays through the CCD electrode structure; photo-absorption in the active layers of the device (i.e. the depletion and field-
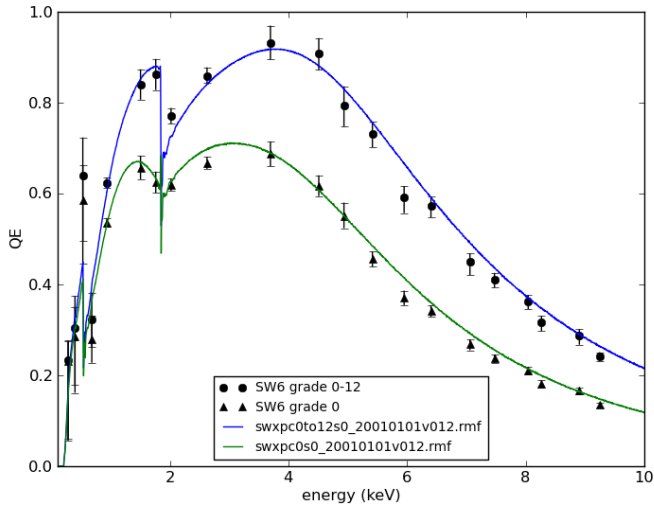
Figure 1: PC mode QE measurements from the *Swift*-XRT flight spare CCD along with the RMF modelled QE.

free regions); charge cloud generation, transportation and spreading; silicon fluorescence and its associated escape peak; surface loss effects; mapping of the resultant charge-cloud to the detector pixel array; charge transfer efficiency; addition of electronic read-out noise; event thresholding and classification according to the specific mode of operation.

Improvements in the RMF code with respect to the previous version include :

- A unified code base for use with both PC and WT modes, only differing by the readout scheme. This now includes exact modelling of the WT readout mode (which clocks 10 parallel rows at a time in the serial register in a continuous process, causing event splitting at the 10-row boundaries), which improves the modelling of the redistribution tail (below ~ 0.4 keV) and 'bump' (between $\sim 0.5 - 1$ keV in grades 1–2) seen in spectra from heavily absorbed sources in this mode.

- Use of the Chandra ACIS Si, SiO_2 and Si_3N_4 linear absorption coefficients when calculating the electrode transmission and Si absorption probabilities and which provide a $\sim 6\%$ deeper Si edge compared with the previous coefficients.

- Modified electrode layer description and thicknesses in order to alter the QE above and below the O-K edge (at 0.545 keV) and improve the modelling of the SNR 1E0102.2–7219 low energy line fluxes.

- Allow differing depletion depths below the open and closed part of the electrode structure.

- Improved surface charge loss function description, with different loss functions under the open and closed part of the electrode. The functional form of these energy dependent loss functions were refined on pre-launch laboratory calibration data at energies corresponding to the Kα lines of C, N, O, F, Al, Si, P, Ti, Fe, and Cu, as well as on post-launch Fe-55 door source calibration data. The loss functions are now interpolated with energy.

- Full field-free and substrate region charge-cloud spreading calculations are now used for both PC and WT modes. The parameters which control the spreading were determined primarily by modelling the post-launch Fe-55 door source data (see below).

- Replication of the ground software (XRTCALCPI) event grading schemes for both PC and WT modes.

The simulated $V_{ss} = 0$ V QE for PC mode was tested against laboratory measurements taken on the XRT flight spare CCD (courtesy of G. Hansford, University of Leicester). Figure 1 shows the measurements and predicted QE for the newly released RMFs, which were generated from simulations assuming a mean depletion depth of 27 microns.

During the post-launch, early in-orbit verification phase of XRT operations the CCD was illuminated by an Fe-55 source located on the camera door. The data, taken before the door opened for science operations, were used to refine the simulation redistribution model for both PC and WT modes and now gives excellent agreement between the data and model (see figure 2).
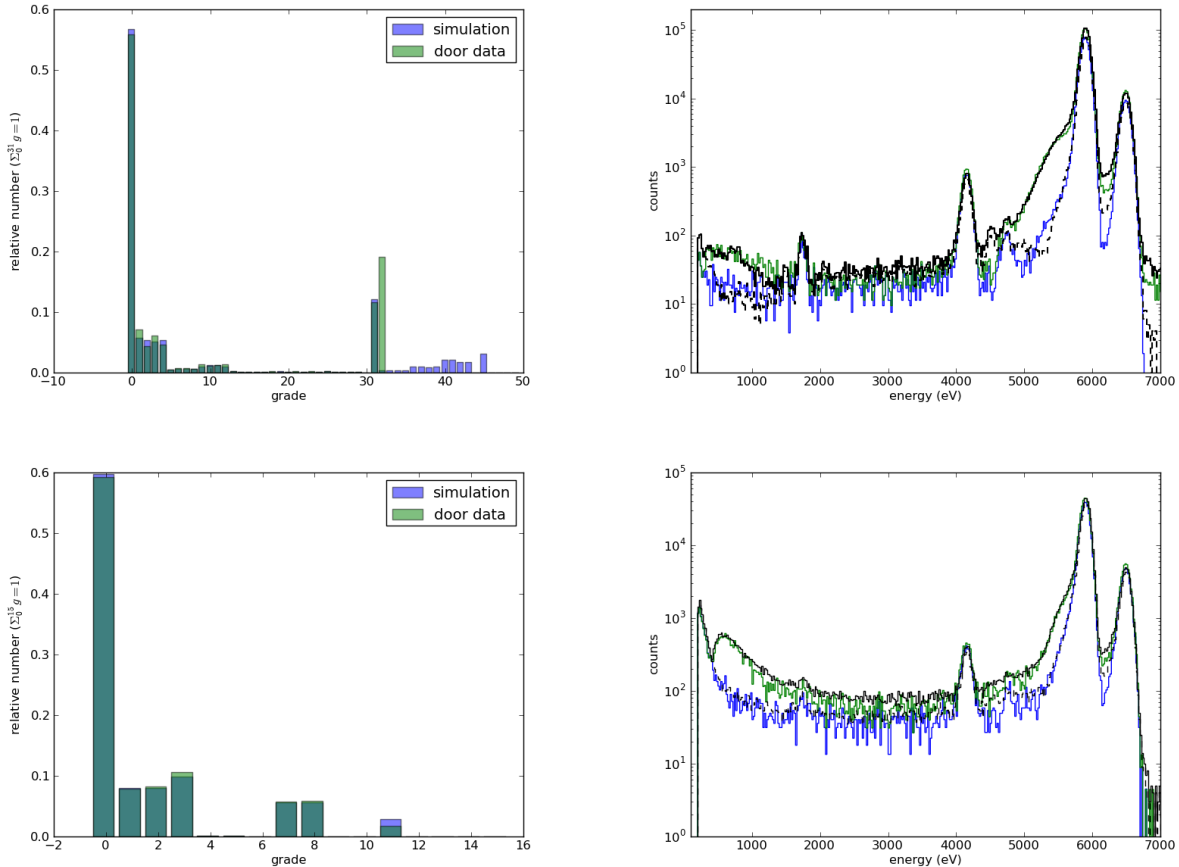
Figure 2: Door source Fe-55 data taken during the early in-orbit XRT verification phase. Top/bottom rows show PC/WT mode, respectively. Left panels show the grade distributions for the data in green and from the simulation code in blue. Right panels show the door source spectra (black solid: grade 0-12 for PC, grade 0-2 for WT; black dashed: grade 0 for both PC and WT) and simulated spectra (green: grade 0-12 for PC, grade 0-2 for WT; blue: grade 0 for both PC and WT).

Due to the overall increase in the charge transfer inefficiency (CTI) and electron noise (EN) levels with time, two sets of RMFs are made available for $V_{ss} = 0\,\mathrm{V}$ observations, with epoch dependent line broadening, modelled by $\mathrm{EN} = 6.75\,e^-$, $\mathrm{CTI_s} = 4 \times 10^{-6}$, $\mathrm{CTI_p} = 8 \times 10^{-6}$ for 2005-Jan to 2006-Dec and $\mathrm{EN} = 8.75\,e^-$, $\mathrm{CTI_{s,p}} = 3.5 \times 10^{-5}$, for 2007-Jan to 2007-Aug (where the subscripts 's' and 'p' refer to the serial and parallel readout directions, respectively).

Ancillary Response Files

Previous XRT ARF releases have required a manual fix to the effective area around the deep Au-$\mathrm{M_V}$ edge (at $2.205\,\mathrm{keV}$). The physical origin behind the correction is thought to be an increase in the mirror reflectivity caused by impurities on the reflecting surfaces.

With this in mind, new on-axis mirror effective area curves were computed by R. Willingale (University of Leicester), which included the effects of a contaminating overcoat layer. The code ray-traces the passage of X-rays through the optical elements of the XRT. These include the 12 concentric gold-coated mirror shells (focal length 3.5 m), the mirror spider support structure (containing 12 spokes) and central optical baffle. The mirror surface roughness was modelled using a power law spectral density function with index -1.4 and integrated roughness of 4.5Å rms. Mirror figuring deformations were also included, although these have only a minor influence on the effective area. The reflecting surface was assumed to be Au, using the optical constants derived by Owens et al. (1996, ApJ, 468, 451), with a thin, uniform overcoat of hydrocarbon contamination (modelled as $\mathrm{CH_2}$). The overcoat increases the reflectivity around the Au-M edges and towards lower energies. A number of mirror area curves were computed for different thicknesses of contaminating overcoat and, together with the filter transmission curves (below), when
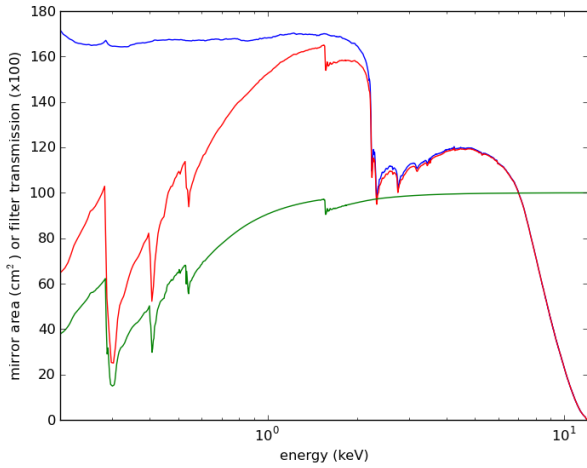
Figure 3: The on-axis ARF file (red) and its associated components (the mirror area curve in blue and the filter transmission curve ($\times 100$) in green).

tested on various in-orbit calibration datasets, gave a preference for a 70Å thick contamination layer.

The optical blocking filter, manufactured by Luxel, is similar to those flown on the *XMM-Newton* EPIC cameras and is composed of a polyimide film coated on one side with a layer of aluminium. Filter transmission data, from both the manufacturer and measured locally at the University of Leicester, were modelled using polyimide and Al mass absorption coefficients provided by M. Barbera (INAF-OAPa; the coefficients were themselves derived from Bessy synchrotron measurements performed on an *XMM-Newton* EPIC medium thickness filter). Due to some uncertainty in the filter transmission measurements and degeneracy in the fitted polyimide and Al layer thickness, a number of transmission curves were produced and, along with the mirror area files (described above), tested on in-orbit calibration data. The tests suggested a filter comprising 2120Å of polyimide and 475Å of Al agree best with the data.

The optimum mirror area and filter transmission curves were combined to generate a common ARF for both PC and WT modes (see figure 3).

Comparison with Calibration data

A number of calibration sources are used to verify the XRT calibration and check the level of agreement seen between other X-ray observatories, some results from which follow.

SNR 1E0102.2–7219

The low energy line-rich source SNR 1E0102.2–7219 (see figure 4), with its IACHEC reference model (Plucinsky et al., 2012, SPIE, 8443, 12), was used to improve the modelling of the effective area around the O-K edge (specifically in WT mode; for PC mode, this is compromised by the fact the source is slightly piled-up), as well as to check the intrinsic resolution calibration of the RMF (in both PC and WT mode). For WT mode data taken in 2005-May, the O ($\sim 570\,\mathrm{eV}$ and $\sim 654\,\mathrm{eV}$) and Ne ($\sim 910\,\mathrm{eV}$ and $\sim 1022\,\mathrm{eV}$) line fluxes agree to within 5 per cent of the IACHEC reference values.

RX J1856.5–3754

The isolated neutron star RX J1856.5–3754 is considered a stable, soft X-ray source, modelled as a 63 eV blackbody (e.g. Beuermann et al., 2006, A&A, 458, 541). The relative normalisation of the model when applied to grade 0 data from different observational epochs is:

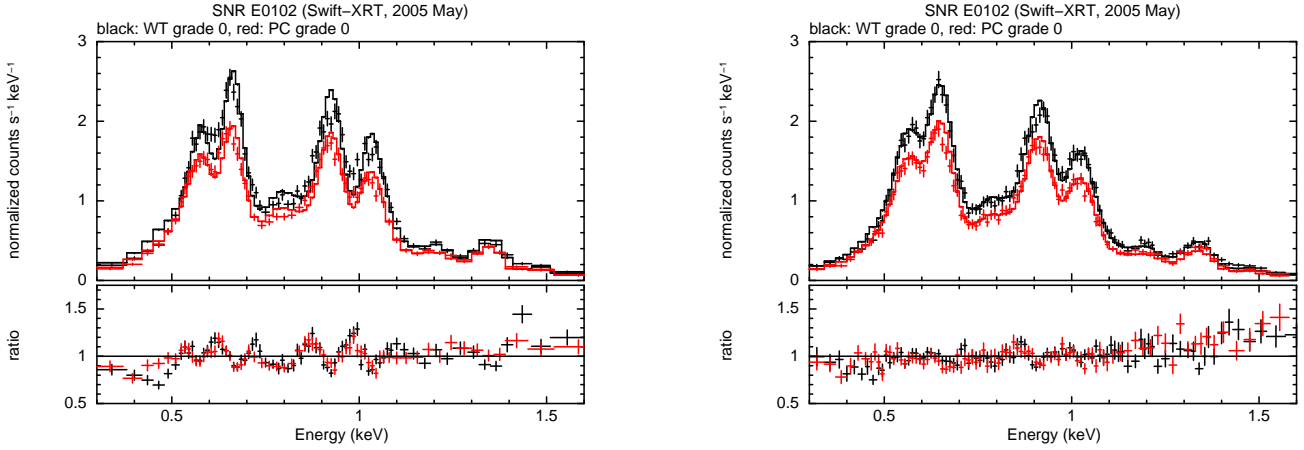|				
2005-Mar :	WT	1.08 ± 0.05,	PC	0.90 ± 0.03
2006-Apr :	WT	0.98 ± 0.03,	PC	0.85 ± 0.03
2007-Jun :	WT	0.86 ± 0.03,	PC	0.77 ± 0.03

Figure 4: SNR 1E0102.2–7219 WT (black) and PC (red) spectra (both grade 0) from 2005-May modelled with the IACHEC reference model. The left figure shows the fit and residuals obtained with the previous v011 RMF/ARF while the figure on the right shows the improvement made to the fit using the new v012 RMF/ARF.

(with uncertainties calculated at $\Delta C = 1$ level). The relative normalisation is seen to slowly decrease by $\sim 15 - 20$ per cent from 2005-March to 2007-June. This is related to a build up of charge traps in the CCD by 2007-June, which effects the low energy response (below $\sim 0.35 - 0.4\,\text{keV}$) the most (as traps cause a significant fraction of charge from low energy X-rays to be lost — or worse, to drop below the event threshold, which is then not recoverable).

Galaxy Clusters

The XRT observed the galaxy clusters Abell 1795, Abell 2029 and PKS 0745–19 in 2005. PC mode spectra were extracted from a $1.5 - 2.5\,\text{arcmin}$ annulus centred on each cluster in order to avoid the cooling flow in the cluster core — at this radius the cluster temperature profile is approximately constant — and extended source ARFs were generated. A similar extraction was performed on *XMM-Newton* pn/MOS data from each cluster. The results (see table 1 and figure 5(a)) show wideband fluxes which agree within 7.5 per cent of the EPIC values, with temperatures $\sim 0.5 - 2\,\text{keV}$ higher.

Table 1: Comparison of XRT PC (grade $0 - 12$), *XMM-Newton* PN (pattern $0 - 4$) and MOS (pattern $(0 - 12)$) spectral fits for the galaxy clusters Abell 1795, Abell 2029 and PKS 0745–19. The spectra were extracted from an $1.5 - 2.5\,\text{arcmin}$ annular region about the cluster centres and extended source ARFs generated. The assumed model is TBABS*APEC (with xsect vern and abund wilm). The uncertainties were calculated at the $\Delta C = 1$ level.

Cluster	$NH_1{}^a$	Instrument	NH^b	kT^c	Ab^d	$F_x{}^e$
Abell 1795	0.12	pn	< 0.001	5.92 ± 0.05	0.56 ± 0.01	1.92 ± 0.01
		MOS1	< 0.03	6.16 ± 0.08	0.58 ± 0.04	1.88 ± 0.01
		MOS2	< 0.002	5.77 ± 0.08	0.52 ± 0.02	1.90 ± 0.01
		XRT-PC	0.165 ± 0.041	7.32 ± 0.43	0.38 ± 0.11	1.76 ± 0.02
Abell 2029	0.33	pn	0.176 ± 0.027	7.95 ± 0.30	0.61 ± 0.09	2.18 ± 0.01
		MOS1	0.322 ± 0.047	8.18 ± 0.42	0.73 ± 0.16	2.19 ± 0.02
		MOS2	0.379 ± 0.047	7.58 ± 0.43	0.47 ± 0.12	2.16 ± 0.02
		XRT-PC	0.421 ± 0.035	9.75 ± 0.46	0.50 ± 0.10	2.03 ± 0.02
PKS 0745–19	4.18	pn	4.465 ± 0.155	9.80 ± 0.79	0.52 ± 0.14	1.24 ± 0.01
		MOS1	5.449 ± 0.202	8.94 ± 0.66	0.62 ± 0.14	1.28 ± 0.01
		MOS2	5.398 ± 0.199	8.19 ± 0.52	0.61 ± 0.13	1.30 ± 0.01
		XRT-PC	5.710 ± 0.160	10.03 ± 0.55	0.75 ± 0.11	1.24 ± 0.01

[a] Galactic (HI) column density; [b] Column density from TBABS ($\times 10^{21}\,\text{cm}^{-2}$); [c] APEC temperature (keV); [d] APEC abundance; [e] $0.3 - 10.0\,\text{keV}$ observed flux ($\times 10^{-11}\,\text{erg}\,\text{cm}^{-2}\,\text{s}^{-1}$).
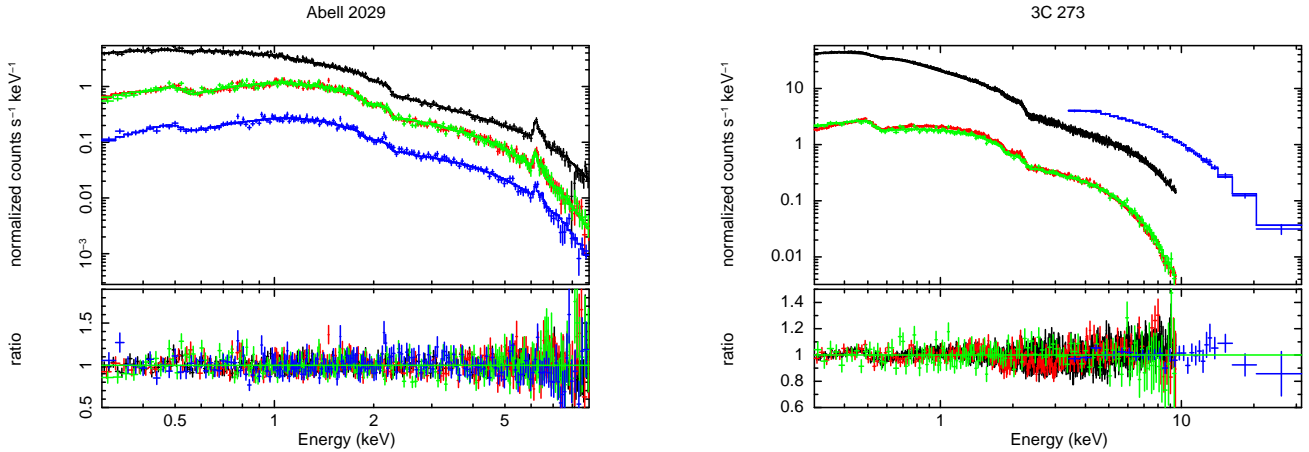
Figure 5: Spectra fit comparisons. Left (a): absorbed single temperature fits to $1.5 - 2.5$ arcminute extracted spectra from Abell 2029 (table 1), showing *XMM-Newton* pn (black), MOS1/2 (red/green) and XRT PC (blue). Right (b): absorbed (powerlaw + zbbody) fits to 3C 273 (table 2), showing *XMM-Newton* pn (black), MOS1 (red), XRT WT (green) and RXTE PCA PCUS 0 & 2 (blue).

SNR G21.5–0.9

The spectrum of the heavily absorbed powerlaw source SNR G21.5–0.9, observed in PC mode in 2006-Aug and 2007-May/Jun, can be well fit with a column density of $3.13 \pm 0.09 \times 10^{22}\,\mathrm{cm}^{-2}$, a photon index of 1.87 ± 0.04 and a $2 - 8\,\mathrm{keV}$ unabsorbed flux of $5.52 \pm 0.07 \times 10^{-9}\,\mathrm{erg\,cm}^{-2}\,\mathrm{s}^{-1}$, in excellent agreement with the cross-calibration work of Tsujimoto et al. (2011, A&A, 525, A25). The measured photon index is ~ 0.1 softer than that returned using the previous V011 CALDB for the same data.

3C 273

XRT WT observations of the quasar 3C 273 were taken contemporaneously with *XMM-Newton* and RXTE on 2005-Jul-10. Spectral comparisons were made over $0.3 - 10.0\,\mathrm{keV}$ for the CCD instruments and $2 - 10\,\mathrm{keV}$ with the RXTE PCA and are shown in table 2 and figure 5(b). The results show fluxes agreeing to better than 10 per cent with the EPIC pn and 5 per cent for the EPIC MOS and RXTE PCA instruments.

Table 2: Cross-calibration results obtained on 3C 273 comparing XRT WT, *XMM-Newton* EPIC and RXTE datasets. The spectra are modelled with TBABS*(POWERLAW + ZBBODY) over $0.3 - 10\,\mathrm{keV}$ and as a powerlaw over $2.0 - 10.0\,\mathrm{keV}$ (with xsect vern and abund wilm). The uncertainties were calculated at the $\Delta C = 1$ level.

Instr	NH[b]	Photon index	kT$_{\mathrm{bb}}$[c]	F$_x$[d]
$0.3 - 10.0\,\mathrm{keV}$[a]				
pn	< 0.005	1.635 ± 0.003	0.123 ± 0.001	1.46 ± 0.01
MOS1	< 0.020	1.598 ± 0.009	0.136 ± 0.005	1.54 ± 0.01
MOS2	< 0.020	1.621 ± 0.008	0.126 ± 0.005	1.57 ± 0.01
XRT WT	0.050 ± 0.050	1.570 ± 0.018	0.122 ± 0.009	1.62 ± 0.02
$2.0 - 10.0\,\mathrm{keV}$[a]				
pn	-	1.579 ± 0.006	-	0.87 ± 0.01
MOS1	-	1.520 ± 0.016	-	0.94 ± 0.01
MOS2	-	1.509 ± 0.016	-	0.96 ± 0.01
XRT WT	-	1.625 ± 0.032	-	0.99 ± 0.02
XTE	-	1.626 ± 0.017	-	1.02 ± 0.01

[a] Fit energy range; [b] Column density ($\times 10^{21}\,\mathrm{cm}^{-2}$) (C.f. expected galactic (HI) column density of $0.17 \times 10^{21}\,\mathrm{cm}^{-2}$); [c] Blackbody temperature (keV); [d] $0.3 - 10.0\,\mathrm{keV}$ or $2 - 10\,\mathrm{keV}$ observed flux ($\times 10^{-11}\,\mathrm{erg\,cm}^{-2}\,\mathrm{s}^{-1}$).

Current limitations and future prospects

Experience has shown that the RMF/ARFs described here can be used reliably over the energy range $0.3 - 10\,\mathrm{keV}$ and return fluxes which agree to within better than 10 per cent when compared with other X-ray missions.

The following considerations apply when using the RMFs/ARFs described here:

- The loss function, which is used by the simulator to describe how charge is incompletely collected from the X-ray interactions occurring near the surface of the device, shifts the redistribution peak of the lowest energy data down in energy. The loss function was derived from pre-launch laboratory calibration data obtained at the University of Leicester, using the central 200×200 pixel region of the detector, in order to be representative of XRT pointings taken close to the on-axis position. At the lowest input energies (C-Kα at $0.277\,\mathrm{keV}$; N-Kα at $0.392\,\mathrm{keV}$), the redistribution is seen to be non-uniform (see figure 6). If a source is positioned outside the central 200×200 region then it might show slightly worse redistribution than modelled by the RMF at the lowest energies (below $\sim 0.4\,\mathrm{keV}$).
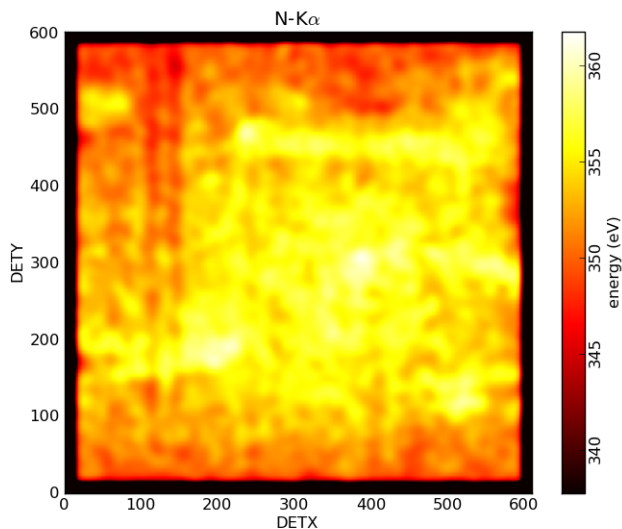

Figure 6: The spatial non-uniformity in the XRT spectral response over the surface of the detector at energies below $\sim 0.4\,\mathrm{keV}$ is illustrated in this image which shows the average event energy for N-Kα ($0.392\,\mathrm{keV}$) photons obtained from pre-launch laboratory calibration data. Event energy shifts of order $10 - 15\,\mathrm{eV}$ are visible outside the central 200×200 pixel region (from within which the response matrix loss function is calculated).

- The soft, blackbody-like source, RX J1856.5–3754 (discussed above), reveals a $15 - 20$ per cent reduction in recovered normalisation (and hence measured flux) when observed in 2007 compared with 2005. This is thought to be due to a build up of charge traps on the CCD by this epoch, which causes low energy events to lose a significant fraction of their input energy, or can even force them to be lost below the event threshold ($0.210\,\mathrm{keV}$, at this time). We plan to investigate whether such $V_{ss} = 0\,\mathrm{V}$ 2007 data can be trap-corrected in the near future. In the meantime, ignoring such data below $\sim 0.35 - 0.4\,\mathrm{keV}$ when fitting can help alleviate the problem.

- High signal-to-noise spectra from sources with featureless continua (such as Mrk 421) typically show residuals of about 3 per cent, for example, near the Au-M$_\mathrm{V}$ edge (at $2.205\,\mathrm{keV}$), the Si-K edge (at $1.839\,\mathrm{keV}$), or the O-K edge (at $0.545\,\mathrm{keV}$). Occasionally, however, residuals nearer the 10 per cent level are seen, especially near the O-K edge, and seem to be caused by small energy scale offsets (caused by inaccurate bias and/or gain corrections). Such residuals can often be improved through careful use of the *gain* command in XSPEC (by allowing the gain offset to vary by $\sim \pm 10 - 20\,\mathrm{eV}$).

- Simulations of WT spectra using a point source illumination model reveal that the redistribution level is dependent on the location of the source on the CCD, as illustrated in figure 7 — a source positioned directly on a 10-row binning boundary experiences a higher fraction of event splitting, which gives rise to slightly heavier redistribution, than one whose vertical position is offset by a few pixels. Differences in the simulated redistribution levels become apparent for column densities above a few $\times 10^{21}\,\mathrm{cm}^{-2}$.

  The new v012 WT RMFs are created assuming the CCD is uniformly illuminated by X-rays. This means there is the potential for slight under or overestimates of the redistributed spectrum towards low energies, depending on the position of the source on the detector and level of absorption seen in the spectrum.

  We plan to evaluate the possibility of releasing source position dependent WT RMFs in the near future.
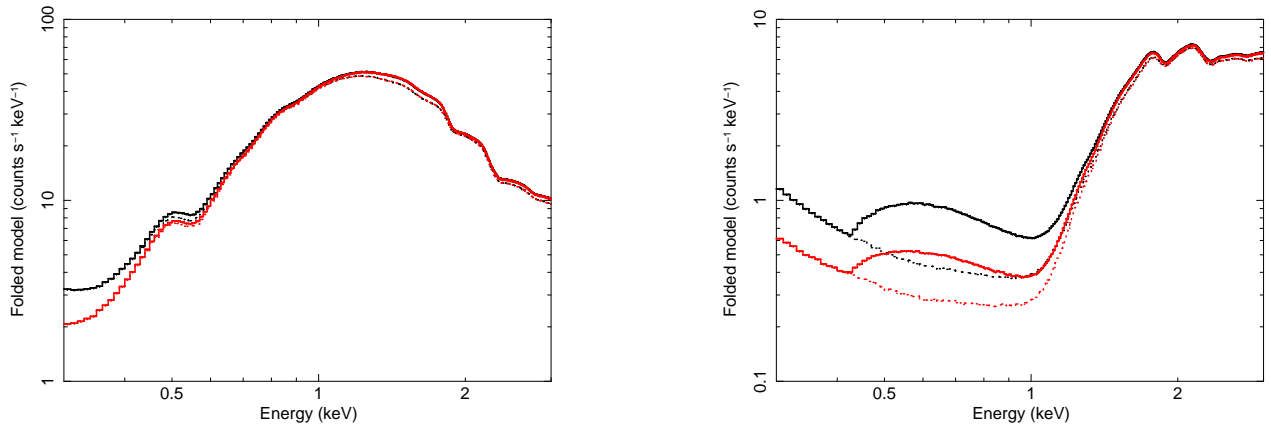
Figure 7: WT simulations of a point source, assuming a $\Gamma = 2$ powerlaw incident spectrum absorbed by 5×10^{21} atoms cm^{-2}, on the left, and 5×10^{22} atoms cm^{-2}, on the right. The black spectra are appropriate for a source located on a WT 10-row binning boundary (in this case at DETY=300.5), while the red spectra are for a source positioned 5 pixels away from the 10-row binning boundary (DETY=305.5). Solid curves show grade $0 - 2$ and dotted curves grade 0. (Note, the grade 0 and grade $0 - 2$ spectra are almost identical in the left panel.)

Summary of RMFs/ARFs currently in use

The following table summarises the RMFs and ARFs available and recommended for XRT spectral analysis and their time dependence.

Table A1: *Swift*-XRT RMFs/ARFs in use as of 2013-Mar-13.

Observation Date		Mode	Grade	File names
From	To			
2004-Dec-01	2006-Dec-31	WT	0-2	swxwt0to2s0_20010101v012.rmf swxs0_20010101v001.arf
			0	swxwt0s0_20010101v012.rmf swxs0_20010101v001.arf
		PC	0-12	swxpc0to12s0_20010101v012.rmf swxs0_20010101v001.arf
			0	swxpc0s0_20010101v012.rmf swxs0_20010101v001.arf
2007-Jan-01	2007-Aug-30	WT	0-2	swxwt0to2s0_20070101v012.rmf swxs0_20010101v001.arf
			0	swxwt0s0_20070101v012.rmf swxs0_20010101v001.arf
		PC	0-12	swxpc0to12s0_20070101v012.rmf swxs0_20010101v001.arf
			0	swxpc0s0_20070101v012.rmf swxs0_20010101v001.arf
Substrate voltage change from 0 V to 6 V on 2007-August-30				
2007-Aug-31	present	WT	0-2	swxwt0to2s6_20010101v014.rmf swxwt0to2s6_20010101v014.arf
			0	swxwt0s6_20010101v014.rmf swxwt0s6_20010101v014.arf
		PC	0-12	swxpc0to12s6_20010101v013.rmf swxpc0to12s6_20010101v013.arf
			0	swxpc0s6_20010101v013.rmf swxpc0s6_20010101v013.arf

Note, the task XRTMKARF automatically reads in the correct ARF from the CALDB, based on information concerning the mode, grade and time of observation contained in the header of the input spectral file. The task also indicates to the screen which RMF is appropriate for the spectrum.

Useful Links

Summary of XRT RMF/ARF releases	http://www.swift.ac.uk/Gain_RMF_releases.html
XRT analysis at GSFC	http://swift.gsfc.nasa.gov/docs/swift/analysis
XRT analysis threads at the UKSSDC, University of Leicester	http://www.swift.ac.uk/XRT.shtml
XRT digest pages at the UKSSDC, University of Leicester	http://www.swift.ac.uk/xrtdigest.shtml
IACHEC website	http://web.mit.edu/iachec/